January 2011

Bystander Attenuation Of Neuronal And Astrocyte Intercellular Communication By Murine Cytomegalovirus Infection Of Glia

Sze Chun Winson Ho
Yale School of Medicine, winson.ho@yale.edu

Bystander attenuation of neuronal and astrocyte intercellular communication by murine cytomegalovirus infection of glia

A Thesis Submitted to the

Yale University School of Medicine

in Partial Fulfillment of the Requirements for the

Degree of Doctor of Medicine

By

Sze Chun Winson Ho

2011

Bystander Attenuation of Neuronal and Astrocyte Intercellular Communication by

Murine Cytomegalovirus Infection of Glia

Abstract

Astrocytes are the first cells infected by murine cytomegalovirus (MCMV) in primary

cultures of brain. These cells play key roles in intercellular signaling and neuronal

development, and they modulate synaptic activity within the nervous system. Using

ratiometric fura-2 digital calcium imaging of >8,000 neurons and glia, we found that

MCMV-infected astrocytes showed an increase in intracellular basal calcium levels

and an enhanced response to neuroactive substances, including glutamate and

ATP, and to high potassium levels. Cultured neurons with no sign of MCMV infection

showed attenuated synaptic signaling after infection of the underlying astrocyte

substrate, and intercellular communication between astrocytes with no sign of

infection was reduced by the presence of infected glia. These bystander effects

would tend to cause further deterioration of cellular communication in the brain in

addition to the problems caused by the loss of directly infected cells.

Table of Contents:

Introduction

Cytomegalovirus (CMV) is a source of significant public health concern. It is a common opportunistic agent of infection in immunocompromised individuals. In immunocompetent pregnant women, CMV infection can lead to congenital infection of the fetus with potentially devastating outcome. Congenital CMV infection can result in serious neurodevelopmental problems ranging from malformation of cortical development, mental retardation, cerebral palsy, to sensorineural hearing loss [1]. These injuries once incurred on the developing nervous system are often irreversible. The mechanism of injury with which CMV causes these significant but variable neurologic sequelae is largely unknown. Understanding the pathogenesis is pivotal in formulating improved modality of treatment and prevention. This project aims to study the impact of CMV infection on the calcium physiology of neurons and astrocytes using in-vitro Fura- 2 calcium imaging of intracellular calcium levels. The murine model was used in this project given the high degree of similarity between the genome of murine CMV and human CMV. The infectious characteristics between human and mouse CMV infection were also comparable [1].

Background

Cytomegalovirus –

CMV is a member of the beta herpesvirus subfamily. It has a double stranded and linear DNA genome of 229 kbp that is largest in the herpes family. CMV is a family of viruses that include species-specific strains that do not cross host species carrier: human (HCMV), mouse (MCMV), chimpanzee (CCMV) and rhesus (RhCMV) [2].

Similar to all herpes virus, CMV infection leads to lifelong latency in the host with intermittent reactivations. In humans, congenital CMV infection occurs through mother-to-child transmission, via either intra-uterine placental transmission or perinatal transmission during delivery or breast-feeding. In contrast to intra-uterine transmission, perinatal infections of full-term babies do not normally result in long-term neurodevelopmental disabilities. Transplacental transmission occurs when pregnant women gain exposure to the virus during gestation. Primary infection occurs when the mother is seronegative for CMV, meaning that the mother has no previous exposure to the virus prior to pregnancy. In non-primary infection, the pregnant woman is seropositive, meaning that the mother is latently infected with CMV and is re-exposed to the virus during pregnancy [1]. The rate of transplacental transmission is higher in primary infection, estimated at between 24-75% [3-6], while the rate of transmission in non-primary infection is 2.2% [3, 5, 6]. However, there is evidence to suggest that the clinical outcome of is more severe in non-primary infection, possibly related to reinfection with a new strain of the CMV virus[3, 7, 8]. CMV is a ubiquitous virus. Age-adjusted prevalence of CMV is about 60%. In children, 0.5-1% acquire in-utero infection, 40% acquire latent infection by the age of 10. By the age of 60, an estimated >80% of the population is infected with the virus[1, 6, 9]. In non-congenital infection of immunocompetent individuals, the virus causes minimal clinical consequence.

Epidemiology of congenital CMV infection –

In the United States, congenital CMV infection accounts for a major cause of birth

defects and childhood disorder. An estimated 0.2-2% of all deliveries, or about 40,000 children, were infected by CMV yearly. An estimated 400 fatalities directly result from congenital CMV infection. At birth, only about 15% of CMV infected babies are symptomatic. Clinical manifestations include intrauterine growth restriction, hepatosplenomegaly, jaundice, thrombocytopenia, microcephaly, periventricular calcifications, and chorioretinitis [2]. About 60-90% of symptomatic infant will have long-term neurologic deficits. An additional 10-15% of asymptomatic children at birth ultimately will develop neurodevelopmental disabilities, which can have variable clinical presentations ranging from mental retardation, psychomotor retardation, hearing loss and ophthalmologic abnormalities[1]. An estimated incidence of 8000 children/year with neurodevelopmental deficits is attributed to congenital CMV infection. To put this in perspective with other prominent causes of congenital birth defects, Down syndrome affects 4000 children/year [1, 7], fetal alcohol syndrome affects 5000 children/year, and spinal bifida affects 3500 children/year [1, 10]. Hence, congenital CMV infection is the most common cause of birth defects and childhood disabilities in the United States.

Diagnosis of in-utero CMV infection –

Given the potentially long-term consequence of congenital CMV infection, accurate diagnosis of CMV infection in pregnancy, especially primary infection, which carries a higher rate of in-utero transmission, is desired. In most cases, CMV infections of pregnant women are asymptotic. Even in the acute phase, less than 5% of mothers demonstrate any symptoms and even fewer have full-blown mononucleosis

syndrome [3]. To diagnosis primary infection, one needs to demonstrate seroconversion, meaning a positive anti-CMV IgM antibody with documented negative test prior to gestation. Since anti-CMV IgM antibodies are not routinely tested, rarely can seroconversion be documented. The presence of anti-CMV IgM alone does not correlate with primary infection, since IgM can be produced in reactivation of latent infection or infection of carrier with new strain. Currently, the most reliable test for primary CMV infection is anti-CMV IgG avidity test. Carrier with latent infection will have high avidity anti-CMV IgG while primary infection will have low anti-CMV IgG. The sensitivity and specificity of the avidity test conducted before 18-week gestation are reported as high as 92-100% and 82-100% respectively [3, 11-15]. For the diagnosis of CMV infection in the newborn, the gold standard is isolation of virus in the urine and/or saliva within first two or three weeks of life. Serologic test for anti-IgM only carry a sensitivity of 70%. Beyond, 2-3 weeks of life, serologic or virologic test do not differentiate between congenital and perinatal infection [3].

CMV Pathology –

The most devastating long-term clinical manifestation of congenital CMV is the irreversible damage on the developing nervous system. The earliest structural abnormalities can be detected by fetal imaging studies at 28 weeks of gestation. Magnetic Resonance Imaging (MRI) or ultrasonogram can demonstrate white matter abnormalities resulting from acute responses of focal necrosis and hemorrhaging. Transvaginal ultrasonograms can demonstrate a range of structural anomalies,

including ventricular adhesions, periventrcular cysts, ependymal protrusions and abnormal sulcations. The pattern of structural abnormalities on fetal imaging studies is useful in determining time and extent of fetal infection, which can have prognostic value [1]. In neonatal and postnatal imagining, children who are symptomatic at birth always are associated with structural brain abnormalities. The most common is intracranial calcification (Fig. 1A). Other changes include ventriculomegaly, polymicrogyria cyst and encephalopathy. In more severe cases, severe malformation of cortical development such as polymicrogyria (Fig. 1B), lissencephaly, porencephaly, and schizencehaly (Fig. 1C) can be seen.

In addition, congenital CMV infection is also the most common cause of nonhereditary sensorineural hearing loss (SNHL), accounting 10-60% of SNHL in children representing 0.2-1.3/1000 live births [1, 16]. SNHL from CMV infection can be clinically apparent at birth or can develop progressively over first several years of life. SNHL has much higher incidence in children who are symptomatic at birth (30-65%) compared to those who are asymptomatic at birth (7-15%). SNHL is frequently the only long-term neurologic sequalae in CMV-infected children who are asymptomatic at birth [1, 17-19].
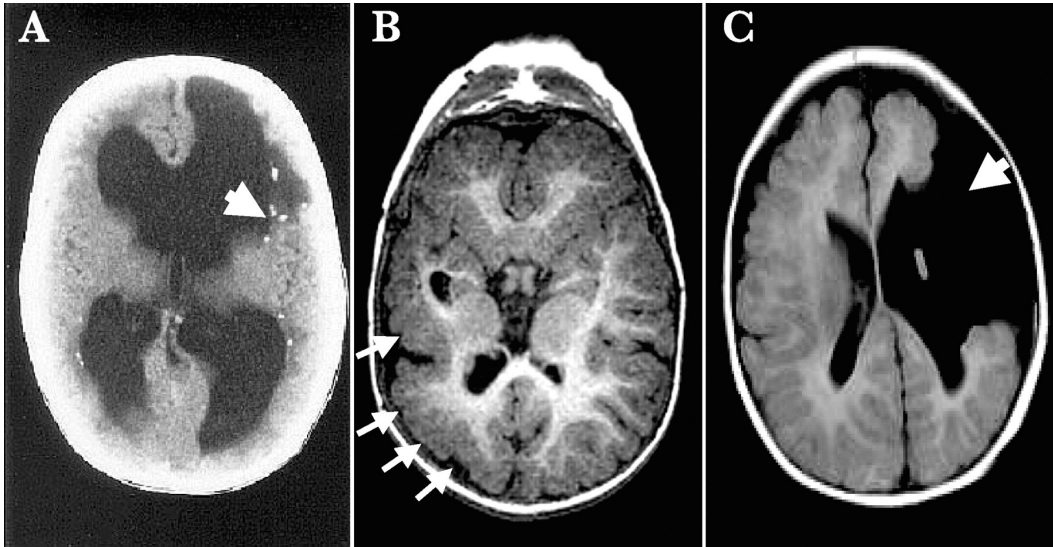
Fig. 1. Examples of neurodevelopmental abnormalities resulting from congenital CMV infection. (A) Computed tomography showing periventricular calcification. Magentic resonance image showing polymicrogyria (B), a neuronal migration abnormality, and schizencephaly with porencephalic cyst. *Adopted from Cheeran et al.*

Calcium Imaging –

Intracellular calcium plays a central role in a wide range of cellular physiological processes, from neuronal signaling, muscular contraction, paracrine exocytosis to apoptosis. Abnormalities in calcium signaling pathways have been implicated in a number of pathologies that affects systems as wide ranging as the nervous, cardiovascular, musculoskeletal to integumentary system [20]. Hence, the study of intracellular Ca2+ can be crucial in understanding the pathophysiological mechanism in a variety of disease processes. The use of fluorescent Ca2+ indicators to study intracellular Ca2+ has been a successful strategy. While there are a variety of Ca2+ indicators, they all share the attribute that their florescent properties shift with Ca2+ binding. Broadly, there are two major categories of Ca2+ indicators: genetically

encoded fluorescent proteins and chemical fluorophores. Genetically encoded florescent proteins require transfection or expression of the Ca2+ sensitive proteins in the cells prior to the experiments, while chemical indicators can be introduced and utilized rapidly [20]. The current project is performed exclusively using the chemical Ca2+ indicator Fura-2.
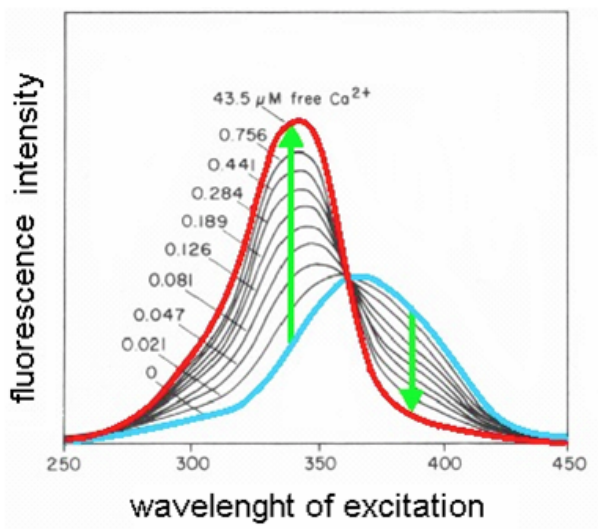

Fig. 2. Intensity of fluorescence plotted against excitation wavelength under different calcium concentrations. At 340 excitation, intensity increase with calcium concentration. At 380 excitation, intensity decrease with calcium concentration.

Fura-2 belong to a special class of chemical Ca2+ indicators known as ratiometric indicators. It has the special property that with Ca2+ binding the excitation spectrum changes. Specifically, the peak excitation absorbance shift from 380 in a Ca2+ free state to 340 nm in a Ca2+ bound state (Fig. 2). This allows for an accurate quantification of Ca2+ level based on the ratio of the fluorescent emission intensity at 340 and 380 excitation. This ratiometric quantity corrects for uneven dye loading, photobleaching, and changes in cellular volume. Hence, the use of Fura-2 allows the comparison of absolute Ca2+ level between different cells. This is property that is crucial in the experiments performed in the current project.

10

Astroctyes and neuronal Ca2+ physiology –

It has been shown previously that MCMV preferentially targets astrocytes in early stages of infection [21]. In the past years, the traditional view that astrocytes in the brain merely provide structural support for neurons has given way to the realization that astrocytes play critical and active roles in processing information, communicating with other glia, and modulating synaptic communication [22-24]. Astrocytes respond to and release transmitters such as glutamate and extracellular ATP through increases in intracellular Ca^{2+} [25-28]. Astrocytes modulate synaptic activity and respond to the release of transmitters from neurons [25, 27, 29, 30]. Astrocytes communicate with one another; intercellular Ca^{2+} elevations initiated in a single astrocyte can propagate to neighboring cells in a wavelike manner mediated by ATP release and enhanced by gap junctions [31-36]. Long-distance intercellular calcium waves occur spontaneously or are triggered by neurotransmitters such as ATP [28, 31] and glutamate [33, 37, 38]. In addition, astrocytes actively modulate synaptic transmission between neurons [30, 37, 39-42]. As astrocyte signaling plays a role in microglia activation and neurogenesis, the preferential MCMV affinity for astrocytes may play a crucial role in the pathogenesis of MCMV, and, therefore, understanding the impact of MCMV on astrocyte signaling may contribute to a greater understanding of the disease process. Although we are unaware of studies investigating ion shifts due to MCMV infection of brain cells, CMV infections of fibroblasts may increase cytoplasmic calcium, thereby possibly enhancing CMV replication [43]. In the present study, we examined the changes in astrocyte Ca^{2+} responses to glutamate, ATP, and depolarization by high K^+ in the course of MCMV

infection. We also tested the hypothesis that infection of the underlying astrocyte substrate alters synaptic communication among co-cultured neurons. Finally, we examined whether intercellular Ca^{2+} waves between communicating glia are impeded by MCMV infection.

Specific Aim:

To study how calcium physiology is altered in mice astrocytes and neurons with MCMV infection using Fura-2 calcium imaging. Specifically, the Ca2+ responses in astrocytes to stimulation with glutamate, ATP and high K+ will be compared in different stages of MCMV infection. Neuronal synaptic activity will be compared between neurons with MCMV infected astrocytes substrate and control. Finally, calcium waves stimulated by mechanical stimulation will be compared between MCMV infected and non-infected astrocytes.

Materials and Methods:

Tissue Culture (this part of the experiment is performed with the help of Dr. Yang, post-doc fellow in the lab) –

Primary cultures were prepared from Swiss albino mouse brains harvested on postnatal day 5 and on embryonic day 17 for astrocyte and neuron preparations, respectively. Care was used to ensure that all cultures used in a particular comparison were of the same age and cell density. The brain tissue was harvested and placed in standard minimal essential culture media (GIBCO) and washed three times. The tissue was then enzymatically digested in Earl's balanced salt solution

containing papain (10 units/ml) and l-cysteine (0.2 mg/ml) for 30 min. The tissue was pelleted and the protease solution was removed by aspiration. The tissue was triturated into a single-cell suspension in tissue culture medium [glutamate- and glutamine-free Dulbecco's modified Eagle's medium (DMEM) supplemented with 10% fetal bovine serum, 100 units/ml penicillin/streptomycin and 6 gm/l glucose]. The suspended cells were plated onto poly-d-lysine (540,000 Da) coated glass coverslips (22 mm^2). For astrocyte-only cultures, the cells were maintained in vitro with minimal essential medium for up to 2 to 3 weeks before use. For high-density neuronal cultures, cells we plated within a 7-mm glass cylinder placed on top of the coverslip. The glass cylinder was removed 60 min after plating. Cytosine arabinofuranoside (2 μM) was then added to the tissue culture medium on the second day in culture to inhibit glial cell proliferation. Cell cultures were maintained at 37°C and 5% CO_2 in a Napco 5410 incubator.

MCMV –

Two different MCMV was used in the current project: a commercially purchased wild-type MCMV (Smith strain; ATCC), and a recombinant MCMV with enhanced Green Fluorescence Protein (GFP) expression, allowing identification of infected cells. GFP transcription was driven by an elongation factor 1a promoter, placed at the IE2 site, a site that did not alter viral replication or tissue preference. GFP expression could be found in infected brain cells within 6 h of CMV inoculation [44].
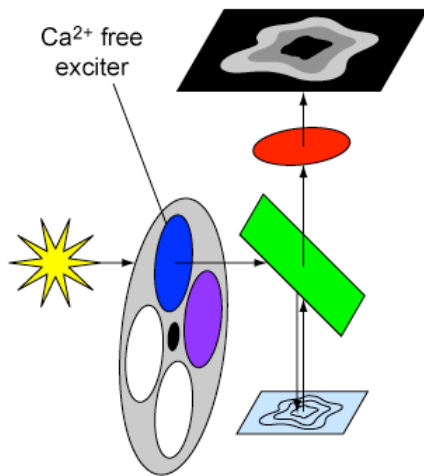
Fig. 3. Calcium imaging experimental setup. A computer controlled shutter wheel alters between 340 and 380 excitation. Ratiometric image can be calculated using those two images and calibrated to an absolute Ca 2+ level.

Calcium imaging –

Fura-2 ratiometric calcium imaging was employed to monitor intracellular calcium levels. Cells were incubated with 5 µM fura-2 acetoxymethyl ester for 30 min at 37°C in standard HEPES buffer solution (10 HEPES, 137 mM NaCl, 25 mM glucose, 5 mM KCl, 1 mM $MgCl_2$, 3 mM $CaCl_2$, pH 7.4). Cultures growing on glass coverslips were then loaded into a laminar-flow perfusion chamber for image acquisition. Ratiometric images were taken every 3 seconds by alternating between 340-nm and 380-nm excitation wavelengths using a Sutter filter wheel controlled by a Sutter Lambda 10-2 microprocessor (Fig. 3). Ratiometric values were then calibrated to Ca^{2+} with a standard curve established using a fura-2 calcium calibration kit (Invitrogen). Images were acquired using a QImaging Retiga EX digital camera and processed with Openlab and IGOR Pro software running on an Apple G5 computer. In some cases, image contrast was corrected by using Adobe Photoshop; all images

in a set were treated simultaneously and in the same fashion to avoid data bias. Ca2+ level of individual cells was inferred by selecting regions of interests in the field of view and the Ca2+ level of each cell can be monitored over the course of the time-lapse recording simultaneously.

Basal Ca2+ -

To assess the change in basal calcium levels of astrocytes with MCMV infection, cultures enriched in astrocytes were infected with MCMV (2.5×10^4 PFU/ml). We recorded the basal Ca^{2+} level at 2 and 3 days postinfection (dpi) of over thousands of astrocytes. Comparison was made between the basal Ca2+ of infected astrocytes with non-infected controls. To assess if the degree of basal Ca2+ change is dependent on viral load, two different doses, Multiplicity of Infection (MOI) of 1 and 5, were used to compare change in basal Ca2+ with noninfected controls. MOI was based on estimating culture cell density by counting number of cells in three high field view and extrapolating the total number of cells in the culture dish. MOI of 1 represents a viral dosage with a one-to-one viron to cell ratio, while MOI of 5 represents a five-to-one ratio.

Astrocyte Ca2+ response to stimulation –

The change in astrocyte Ca2+ response to stimulation with glutamate (100 µM), high K^+ (55 mM), and ATP (10 µM), was assessed. Stimulation was performed by changing the perfusion buffer of the chamber with the desired stimulus. An infection dose of 0.5 MOI was used for these experiments. The Ca2+ responses to these

stimuli were assessed at two different time points of infection, 2DPI and 3 DPI, and were compared to non-infected controls. Ca2+ response was calculated by subtracting the basal Ca2+ (average of 20 seconds of Ca2+ level before stimulation started) from the stimulated Ca2+ (average of 20 seconds of Ca2+ after stimulation started).

Bystander effect on neuronal synaptic activity –

To test the hypothesis that MCMV infection of astrocytes may change neuronal communication, mixed astrocyte-neuron cultures were infected with low levels of MCMV-GFP (MOI 0.5). Experiments were performed at a time when there was clear infection of the underlying astrocytes but little or no infection of the overlaying neurons. The cells were electrically stimulated (ES) using electrodes on opposite edges of the recording chamber with a Grass SD9 stimulator. A rise in Ca^{2+} levels was triggered by passing a current of 0.06 V/mm^2 through the chamber for 3 ms at 7 Hz. To demonstrate that the observed rise in Ca2+ was a result of activated synaptic activity of neurons, ES under tetrodotoxin (TTX) at 10 uM or ionotropic glutamate receptor antagonists (AP5 [dl-2-amino-5-phosphonopentanoic acid] at 100 µM and CNQX [6-cyano-7-nitroquinoxaline-2,3-dione] at 10 µM) was used to chemically block the ability of neurons to conduct action potential. ES under such conditions was used to show if the ES-dependent Ca2+ rise was dependent on neuronal synaptic activity and not direct activation of voltage Ca2+ channels.

Calcium Waves –

To examine how MCMV infection alters the propagation of glial waves. Astrocyte-enriched cultures were infected with GFP-MCMV at MOI of 1. Experiments were conducted at 2 dpi when there some percentage of astrocytes had clear GFP expression. Calcium waves in astrocyte-enriched cultures were triggered by light mechanical stimulation with a glass pipette that led to an intercellular Ca^{2+} wave. The impact of infection was assessed by examining 3 distinct properties of the wave: total distance traveled, total number of cells involved and propagation velocity. Total distance of waves was measured by the greatest radial distance between the point of stimulation and the furthest point of Ca2+ increase. The total number of cells was tallied by counting the number of cells with Ca2+ after stimulation. Maximum wave velocity was assessed by the largest distance traveled between each frame of the acquisition during wave propagation. A large number of wave samples was collected to make a collective comparison between infected cultures and noninfected controls.

Results

Basal Ca+ changes - We monitored the basal Ca^{2+} level at 2 and 3 days postinfection (dpi) and found an increase from a Ca^{2+} level of 105 ± 1 nM (mean ± standard error) in noninfected controls to 146 ± 3 nM in MCMV-infected cells at 3 dpi (n = 4,050, P < 0.05, analysis of variance [ANOVA] with the Bonferroni procedure) (Fig. 3A). In a separate experiment, we examined the changes in the basal Ca^{2+} levels by using different concentrations of the virus. Basal Ca^{2+} levels at 1 dpi showed an increase from 125 ± 1.9 nM in control cells (n = 658) to 132 ± 2.1 nM at a

multiplicity of infection (MOI) of 1 (n = 605, P < 0.05) and to 221 ± 2.7 nM at an MOI of 5 (n = 811, P < 0.01). To avoid minor differences in Ca^{2+} responses from one region of the coverslip to another, each group is based on more than six imaging regions from two to four coverslips.
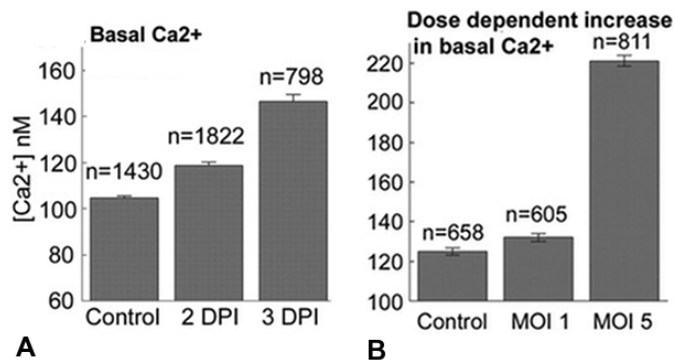
Fig. 3. (A) The mean basal intracellular Ca^{2+} level in astrocytes is increased by MCMV at 2 and 3 dpi. (B) The mean basal intracellular Ca^{2+} increase in astrocytes is dependent on viral concentration.

Fig. 4A-B. Typical raw 340-nm and 380-nm excitation images and ratiometric images of 340/380 calibrated to Ca^{2+} in pseudocolor show a color spectrum from blue (representing low Ca^{2+}) to red (representing high Ca^{2+}) of uninfected and infected cells, respectively (scale bar, 50 μm).

Fig. 5A-B. Representative Ca^{2+} traces of astrocyte responses to glutamate (Glut), a high level of K$^+$, and ATP in uninfected (A) and infected (B) cells.
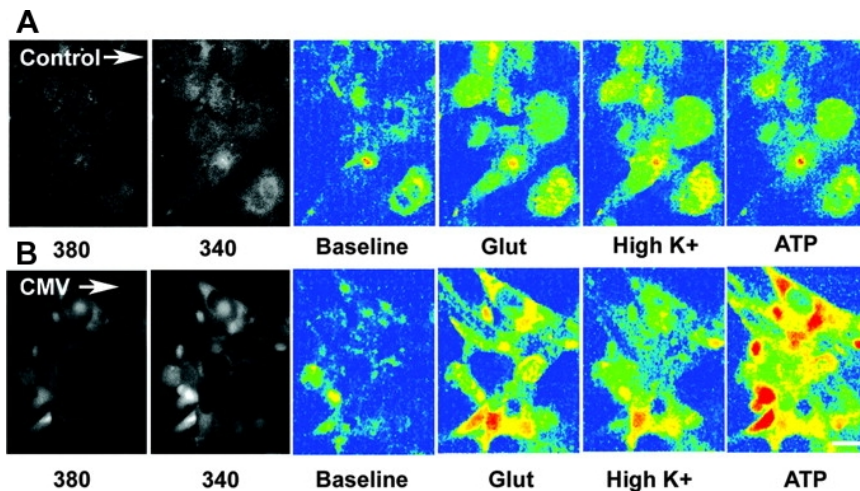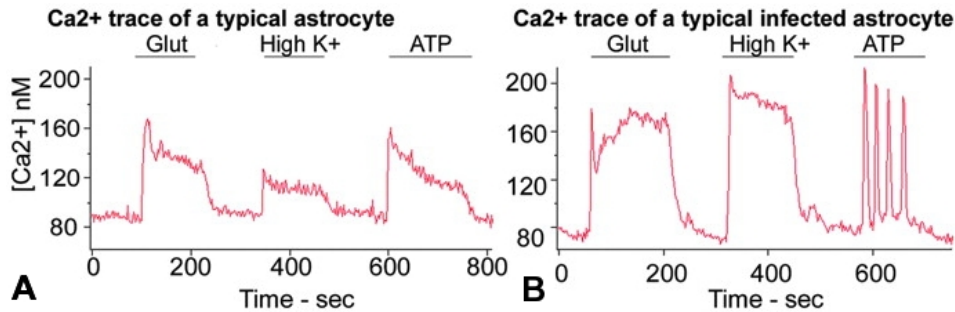
Astrocyte Ca2+ response to stimulation –

Calcium responses to stimulation by glutamate (100 µM), high K$^+$ (55 mM), and ATP (10 µM) were examined in astrocytes infected with wild-type MCMV at MOI 0.5. In Fig. 4 typical raw 340-nm and 380-nm excitation images and ratiometric images of 340/380 calibrated to Ca^{2+} were shown for uninfected (Fig. 4A) and infected (Fig.4B) cells. Calcium levels of individual cells were graphed by selecting regions of interest corresponding to each cell in the calibrated images. Representative traces of Ca2+ changes in response to glutamate, high K+ and ATP are shown in Fig. 5. Responses in uninfected controls, infected cells at 2 dpi and 3dpi were examined. At 2 dpi, MCMV infected astrocytes showed a greater rise in intracellular calcium concentration than did noninfected control cells when stimulated with ATP (Fig. 6A), high K$^+$ (Fig. 6B) and glutamate (Fig. 6C) suggesting that MCMV enhances the calcium response to a number of neuroactive substances (*n* = 1,088, *P* < 0.05, ANOVA with Bonferroni procedure); only responding cells were included in the data means. This finding is interesting as it suggests that the astrocytes become hypersensitive to neurotransmitter stimulation in the course of infection. This

sensitization appears to be general to all three agents tested, suggesting an altered sensitivity of the glutamate and extracellular purinergic ATP receptor responses as well as the voltage-gated calcium channels stimulated by high K^+. At 3 dpi, cells no longer showed an exaggerated calcium response to ATP, glutamate, or high K^+. Given the central roles that glutamate and ATP play in intercellular glia-glia and neuron-glia communications [41, 45-47], the altered astrocyte responses to these neurotransmitters may impede normal functioning of the nervous system. The percentage of cells responding to the different stimulations during the course of CMV infection was also examined. The response to ATP was robust, with almost all cells still responding at 3 dpi, whereas the percentage of cells showing a detectable rise in Ca^{2+} levels due to high K^+ and glutamate fell to 66% and 20%, respectively, at 3 dpi (Fig. 6D). This suggests that there is a sequence (glutamate → high K^+ → ATP) in which astrocytes become unresponsive to the three stimulations as infection proceeds. Another notable observation is that in response to ATP, a markedly higher percentage of infected astrocytes show repetitive oscillations in Ca^{2+} levels from 3% ± 0.8% in noninfected control cells to 29% ± 5.1% at 2 dpi (n = 1,006, P < 0.05, two-tailed t test) (Fig. 6E). These oscillations occur in single cells and are characterized by a rise and fall in calcium levels over a period of about 15 s. This suggests that infected cells did not sustain a consistently elevated Ca^{2+} response but, rather, oscillations in the Ca^{2+} response in the form of multiple peaks. At 3 dpi, the oscillations were not sustained and the response to ATP came mostly in a single peak.
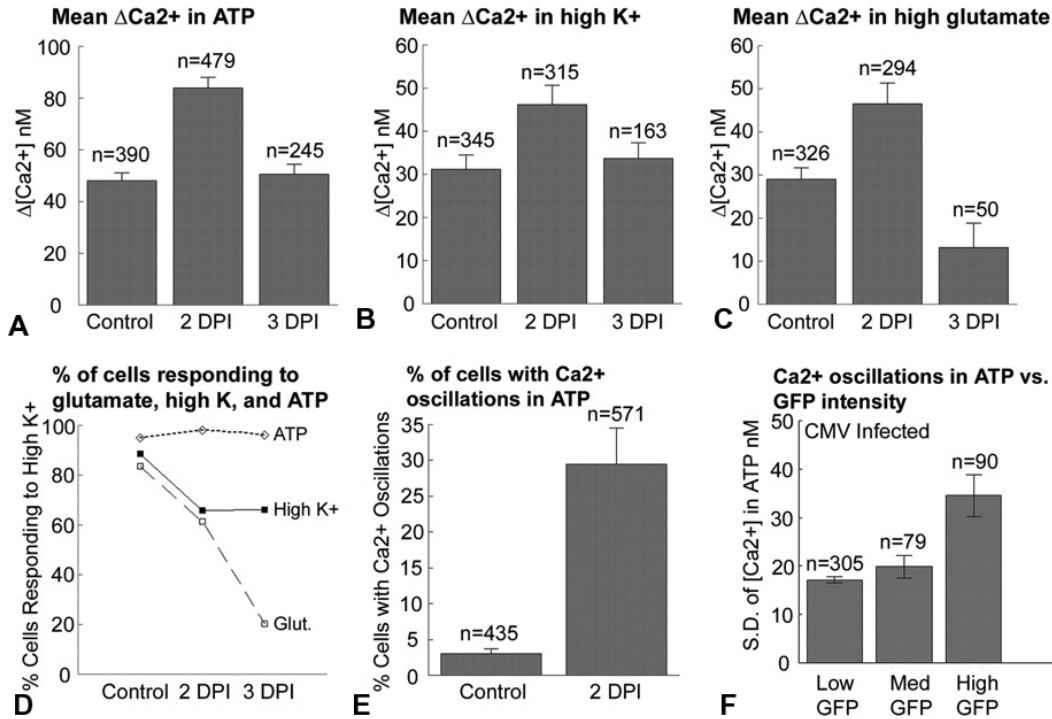
Fig. 6. Change in Ca2+ response to chemical stimulation in MCMV infected astrocytes. At 2 dpi, infected cells show increased responses to ATP (A), a high level of K^+ (B), and glutamate (C). This exaggerated response was lost by 3 dpi. (D) The proportion of cells responding to glutamate (Glut) and a high level of K^+ decreased at 2 and 3 dpi. However, almost all cells retained responsiveness to ATP stimulation. (K) The percentage of cells displaying a high level of oscillations in Ca^{2+} concentration during ATP stimulation increased after infection. (L) Using a GFP-expressing MCMV, the degree of Ca^{2+} concentration oscillations in response to ATP as determined by the standard deviation of Ca^{2+} concentration is correlated with GFP intensity, suggesting that increased levels of MCMV infection are correlated with a greater degree of Ca^{2+} oscillations.

Using the recombinant GFP-MCMV strain, the detection of MCMV infection was correlated with the expression of the reporter gene. In a separate experiment in which astrocytes were infected with the MCMV-GFP strain, cells were divided into three groups based on the measured fluorescence intensity of the GFP signal, determined by using a 12-bit digital camera (low, 0 to 500; medium, 500 to 1,500;

21

and high, 1,500 to 4,095). The level of Ca^{2+} oscillations, based on the standard deviation in Ca^{2+} concentration under ATP perfusion, showed a statistically significant increase in the high-GFP group compared to the low- or medium-GFP groups (n = 474, P < 0.05, ANOVA with the Bonferroni procedure) (Fig. 6E), suggesting that cells with a higher level of infection showed more oscillations in calcium level. Glial Ca^{2+} oscillations may serve to orchestrate the release of, or response to, transmitters [30, 48].

In order to preclude the possibility that the observed changes in calcium levels were due to factors other than the process of MCMV infection, two control experiments were performed. Using MCMV-GFP, the basal Ca^{2+} levels of uninfected cells in infected mouse astrocyte cultures (2 dpi), selected by the absence of a GFP signal, were compared to those of noninfected control cultures. At 2 dpi, the mean basal Ca^{2+} level did not increase in the uninfected cells of infected cultures compared to that of the control cultures; mean Ca^{2+} concentrations were 169 ± 7 nM (n = 253) and 141 ± 19 nM (n = 151), respectively (P = 0.28). In a second control experiment, MCMV-GFP, inactivated with UV light for 5 h, was used to compare the Ca^{2+} responses of astrocytes to high K^+ levels and ATP. At 2 dpi, responses in cultures inoculated with the inactivated virus showed no increase compared to the control: mean Ca^{2+} levels in response to high levels of K^+ were 313 ± 12 nM (n = 127) in inoculated cells and 298 ± 13 nM in control cells (n = 113); the mean Ca^{2+} levels in response to ATP were 504 ± 22 nM (n = 134) in inoculated cells and 497 ± 20 nM in control cells (n = 113, P = 0.78). Inactivation was confirmed by the failure of MCMV-

GFP to express GFP in any cell, while the same amount of virus before UV treatment did express GFP at the same dpi. These experiments suggest that changes in Ca^{2+} levels are not attributable to contaminants in the inoculum but rather that active replicating virus is responsible. In addition, it is also shown that the MCMV-mediated increase in Ca^{2+} increase occurs selectively in infected astrocytes and not in bystander astrocytes in the same dish.

Neuron response to electrical stimulation is eliminated by TTX
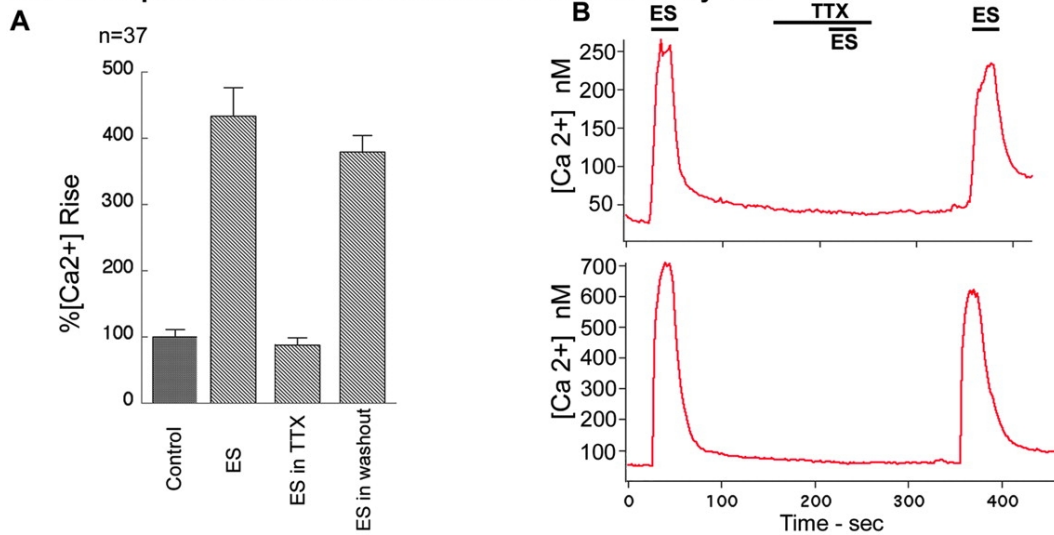
Fig. 7. (A) In the presence of TTX, the neuron response to ES is completely abolished. This indicates that the Ca^{2+} increase in response to ES is attributed to an increase in synaptic activity and not to the direct activation of voltage-gated Ca^{2+} channels, supporting the use of the ES response as a measure of synaptic activation. The ES response recovered after the washout of TTX. (B) Two representative Ca^{2+} traces showing a complete block of the ES response in the presence of TTX as well as the recovery after the TTX washout.

Bystander effect on neuronal synaptic activity –

To address the question of whether neuronal synaptic activity is affected by MCMV infection of underlying astrocytes independent of infection of the neurons themselves, GFP-MCMV at MOI of 0.5 was used to infect mixed astrocyte-neuron cultures. As expected from known trophism of MCMV infection, astroctyes become preferentially infected at early stage of infection. As shown in Fig. 8B GFP expression comes exclusively from the astrocytes, not from neurons, in a field with high density for both cell types. In the presence of tetrodotoxin (TTX) to block spike-mediated transmitter releases, the electrically stimulated Ca^{2+} rise was completely eliminated (Fig. 7). Similarly, the ionotropic glutamate receptor antagonists (AP5 [dl-2-amino-5-phosphonopentanoic acid] at 100 µM and CNQX [6-cyano-7-nitroquinoxaline-2,3-dione] at 10 µM) blocked the stimulated response (not shown). Fig. 8 shows that the synaptic activity of neurons with infected underlying astrocytes becomes attenuated in comparison to that of the control cells. MCMV infection of astrocytes reduced the ES-mediated Ca^{2+} rise in neurons from 176 ± 6 nM in control cells to 131 ± 6 nM (n = 907, P < 0.05, two-tailed t test), suggesting that MCMV altered neuronal communication by the infection of astrocytes, even before the neurons showed any sign of infection. Since TTX blocks spike-mediated neurotransmitter release and glutamate receptor antagonists block the response to synaptic glutamate release, together these data support the view that the electrically evoked calcium rise is due to the synaptic release of glutamate and not to a direct effect of electrical stimulation on voltage-gated calcium channels.

Fig.8D shows an additional control in which neuron-enriched cultures, in the

absence of an underlying astrocyte substrate, were inoculated with the MCMV at the same MOI as that described above. When used for calcium imaging, neurons did not show GFP expression or a cytopathic effect. This allows for the possibility that there may be a low level of infection of neurons that was not detected by measuring GFP expression and that could potentially alter neuronal signaling. Electrically evoked and synaptically mediated calcium level increases did not differ between control and MCMV-inoculated cultures; the change in Ca^{2+} level was +76 ± 4 nM in control cultures and +81 ± 4 nM in MCMV-inoculated cultures (n = 801, P > 0.3, two-tailed t test). This supports the view that an infected-astrocyte substrate is most likely responsible for the attenuation of neuronal synaptic communication.
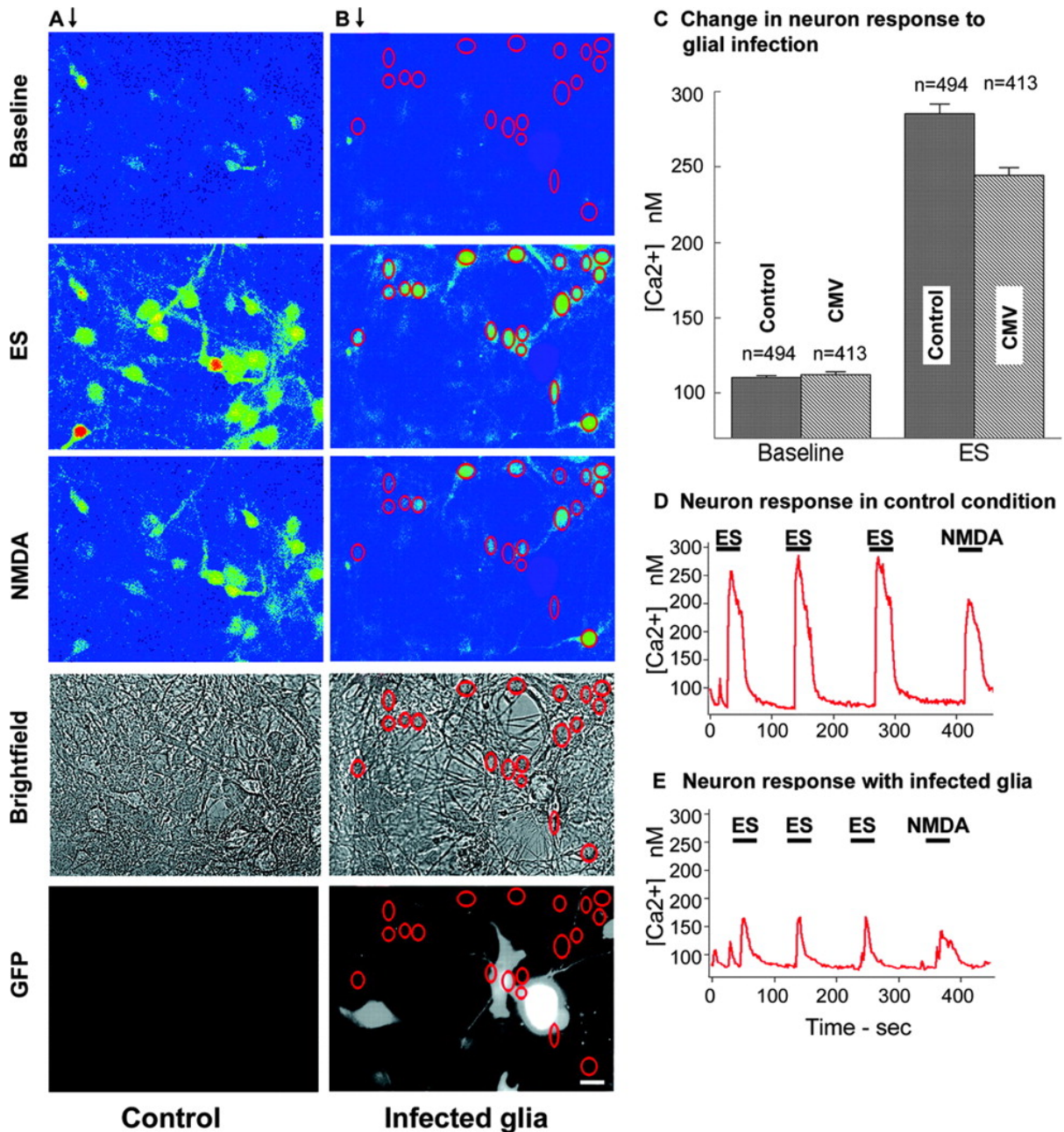
Fig. 8. Astrocyte infection reduces neuron synaptic responses. (A and B) Ratiometric images of 340/380 nm calibrated to Ca^{2+} show neuronal responses to ES and *N*-methyl-D-aspartic acid (NMDA). Synaptically linked neurons are identified by their responsiveness to both ES and NMDA, with confirmation based on morphology in brightfield images. The GFP intensity indicates the level of MCMV infection. Cells in red circles in panels B are neurons responding to ES and NMDA that are uninfected by MCMV as shown by the absence of GFP signal. Underlying astrocytes are, however, heavily infected, and show a bright GFP signal. Scale bar, 20 μm. (C) The change in the ES response

of neurons on infected astrocytes was lower than that on control neurons growing with uninfected astrocytes. The change in Ca^{2+} concentration decreased from 175 ± 6 nM in control cells to 132 ± 6 nM in neurons with infected astrocytes. (D and E) Representative Ca^{2+} traces of neurons responding to ES and NMDA with normal astrocytes (D) and with MCMV-infected astrocytes (E).

No change in neuron response to electrical stimulation in inoculated culture without glial infection
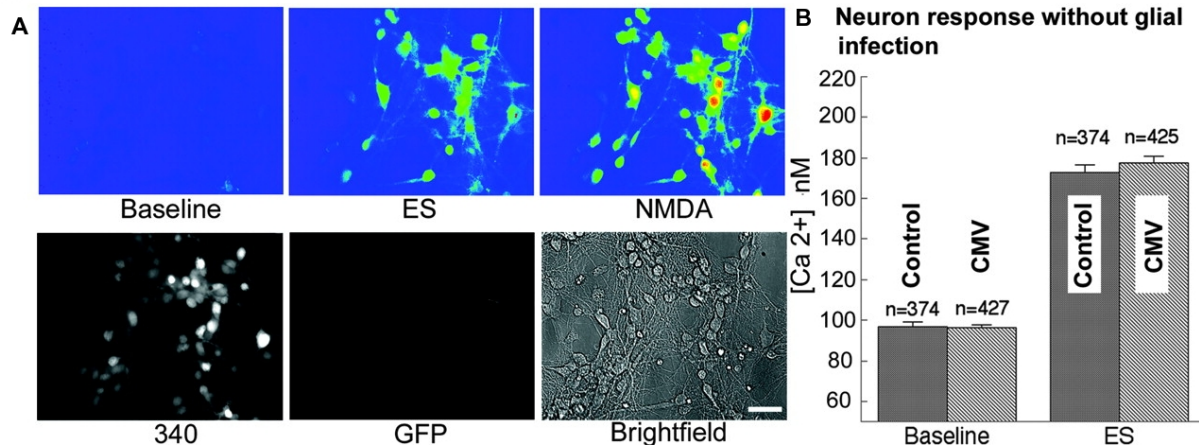
Fig. 8. (A) Ratiometric images of 340/380 nm calibrated to Ca^{2+} showing the neuronal responses to ES and NMDA (*N*-methyl-D-aspartic acid). The 340-nm and brightfield images show the absence of underlying astrocytes; the GFP image shows that the experiment is performed at a time when no MCMV reporter gene expression or cytopathic effect can be detected. Scale bar, 30 μm. (B) The mean ES response of neurons is unchanged in the absence of astrocyte infection.

Calcium Wave –

The effect of infection on the propagation of glial wave conducted by astrocytes was examined. Three properties of glial waves were studied: total distance travelled, total number of cells involved and maximum wave velocity. In Fig.9A-C, we demonstrated the glial waves triggered by mechanical stimulation in noninfected controls and MCMV infected astrocytes. MCMV infection strongly attenuated calcium wave propagation. In MCMV-infected astrocytes, the mean distance traveled in a single

triggered wave decreased from 434 ± 36 µm to 119 ± 23 µm, the mean number of cells in a wave decreased from 53 ± 5 cells to 19 ± 2 cells, and the maximum propagation velocity dropped from 15 ± 3 µm/s to 8 ± 1 µm/s ($n = 54$, $P < 0.05$, two-tailed t test) (Fig. 9D-F). Given that glutamate and ATP are critical messengers in the propagation of calcium waves, it is possible that the change in the responses to ATP and glutamate described earlier contributes to the disruption of wave propagation. Fig. 9C also shows an interesting consequence of MCMV infection on the spatial distribution of waves in infected cells. Wave propagation is spatially limited by infected cells, demonstrating that those cells can form a barrier between astrocytes with no sign of infection, over which wave propagation is attenuated. To test further the effect of infection on intercellular glial signaling, astrocytes were grown in thin strips, and MCMV was focally applied by a micropipette to a single region of each strip. Three days later, noninfected astrocytes were stimulated, and the distance the wave traveled was measured. By focusing only on cells not expressing the MCMV-GFP reporter, calcium waves were found to be strongly attenuated in proximity to infected cells, reducing the distance the wave traveled from 554 ± 19 µm ($n = 6$) when the wave did not encounter infected cells to 264 ± 16 µm ($n = 6$) when the wave met infected glia (not shown). Thus, MCMV reduces the velocity of and distance traveled by calcium waves in astrocytes. Importantly, the intercellular calcium wave is attenuated in astrocytes showing no sign of infection.

A↓ 340
Ratio#1 Origin
Ratio#2
Ratio#3
Ratio#4
Ratio#5
Ratio#6
GFP

Wave in non-Infected glia

Control

B↓ 340
Ratio#1 Origin
Ratio#2
Ratio#3
GFP

Wave in infected glia

C↓ 340
Ratio#1 Origin
Ratio#2
Ratio#3
Ratio#4
GFP

Spread of wave confined by surrounding infected glia

CMV (20Hr PI)

D Total distance traveled by a single wave

Distance -um

n=23 waves
n=31 waves

Control   20Hr PI

E Number of cells involved in a single wave

Number of cells

Control   20Hr PI

F Max. velocity traveled by a single wave
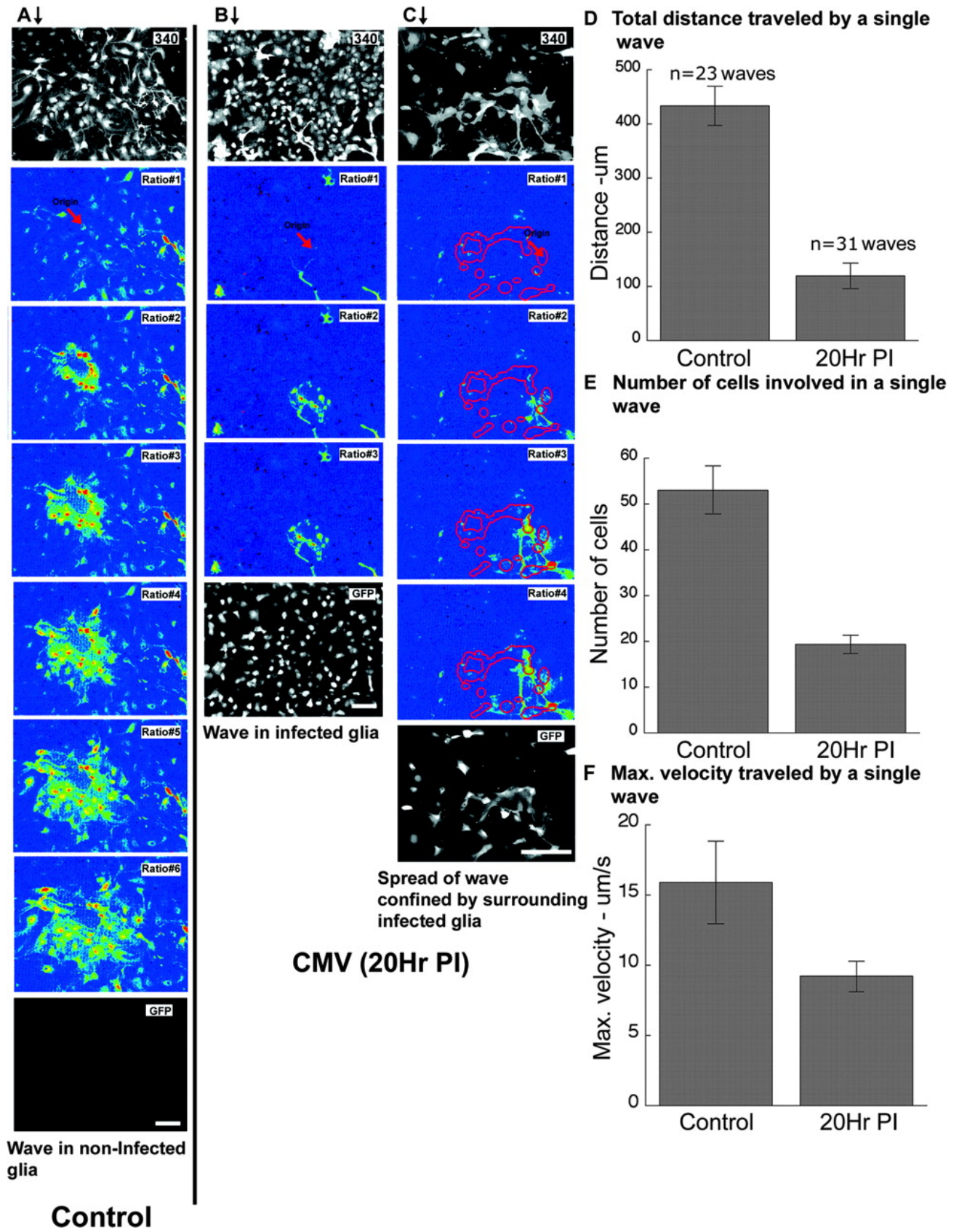
Max. velocity - um/s

Control   20Hr PI

29

FIG. 9. Intercellular Ca^{2+} waves are attenuated by MCMV. (A to C) Sequences of ratiometric images of 340/380 nm excitation in pseudocolor calibrated to Ca^{2+} show the progression of intercellular waves triggered by light mechanical stimulation in uninfected control astrocytes (A) and infected astrocytes (20 h postinfection) (B and C). Red arrows indicate points of stimulation. GFP images show the distribution of infected astrocytes. Intercellular Ca^{2+} waves are significantly inhibited in infected cells. Infected cells spatially confine the spread of a wave in other cells (C). Scale bar, 150 µm. Note that the magnification is higher in panel C than in panels A and B. (D) The mean distance traveled by a wave is decreased in infected astrocytes. (E) The mean number of cells in a wave decreases in infected astrocytes. (F) The maximum velocity traveled by a wave decreases in MCMV-infected astrocytes.

Discussion

In summary, we have reported several observations of how astrocytes and neurons are affected my MCMV infection in an in-vitro model using Fura-2 Calcium imaging. First, we have shown that astrocytes are sensitized to a range of stimulation resulting in hyperexcitability during the course of CMV infection. Second, we have demonstrated that neuronal synaptic activity is attenuated when underlying astrocytes are infected. The attenuation of neuronal communication appears to be a bystander effect secondary to astrocyte infection, since no detectable infection was found in neurons. Third, we have also shown that CMV infection dramatically affects propagation of glia waves activities. To extrapolate the relevance of these observations in-vivo in the setting of congenital CMV infection, one has to review the current understanding of the role astrocytes play in the nervous system. In the last decade, there is a paradigm shift in the concept of the functional importance of astrocytes in neuronal communications. In the past, it was assumed that astrocytes

30

merely form a passive framework that acts as a substrate for overlying neurons. But recent findings suggest that they do a lot more, and the idea of the "tripartite synapse" arose [49] (Fig. 10). A tripartite synapse comprise of the pre- and post-synaptic neurons as well as the glial processes that ensheath the junction [40]. The astrocytes regulate the microenvironment around synapse. It recycles the released glutamate in the form of glutamine to the presynaptic neurons and maintains ion homeostatsis of extracellular K+ concentration and pH [49]. In addition, a new subtype of glial cells, known as the oligodendrocyte precursors cells (OPCs) was recently identified. OPCs express proteoglycan NG2 and distinct physiologic and morphologic characteristic from other glial types [49-51]. OPC have been shown to conduct fast synaptic transmission mediated by GABA or glutamate [49, 52-55], highlighting the possibility of an even more integral role astrocytes play in the neuronal signaling.
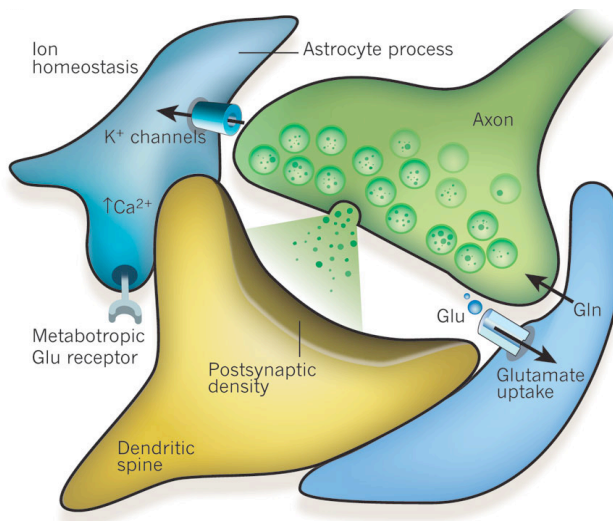
Fig. 10. Schematic representation of a tripartite synapse. Perisynaptic astrocyte (blue cells) processes contain transporters that take up glutamate (Glu, green circles) that has been released into the synapse and return it to neurons in the form of glutamine (Gln). Glutamate receptors on astrocytes sense synaptic glutamate release, which in turn induces a rise in Ca^{2+} concentration in the astrocytes. One of the main functions of glia at the synapse is to maintain ion homeostasis, for example regulating extracellular K^+ concentrations and pH. *Adopted from Eroglu et al[49].*

Glia are known to play an important role in controlling synapses formation and elimination. Neurons cultured in the presence of astrocytes have been shown to have ten times the excitatory synaptic activities and form five- to seven times more synaptic connection than if the neurons are cultured alone [49, 56, 57]. Several studies had also identified three distinct subtypes of signaling factors secreted by glia that regulate the development of glutamate-mediated synapses [49, 58] (Fig. 11). These glia-secreted factors either silent or strengthen synaptic connection by altering density of post-synaptic receptors or the probability of neurotransmitter release pre-synaptically. Glia have also been implicated in regulating axon pruning in the developing nervous system. A recent study suggests that immature astrocytes

secret an unidentified signaling molecule that upregulates expression of neuronal C1q, preferentially in weak synapses that are destined to be removed. C1q is the protein that initiates the classic complement pathway that results in phagocytosis. The mechanism with which the upregulation of C1q protein occurs preferentially in weak synapse is unclear. Once tagged with C1q, microglia cells, which are resident immune cells of the brain that contains C1q receptors on their surface, are likely responsible for removal of unwanted synapses [49].
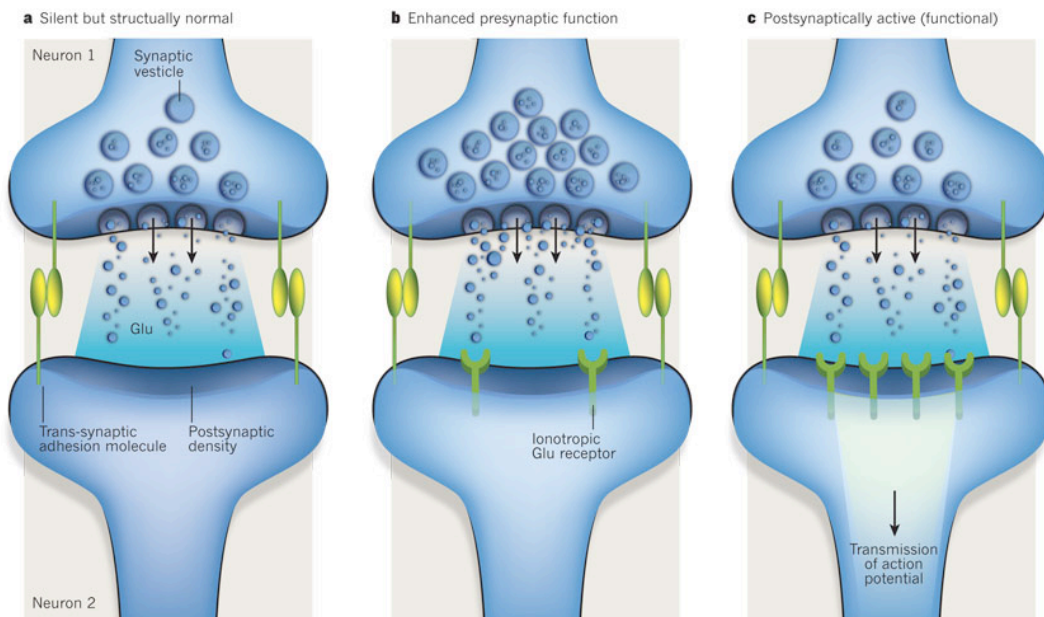
Fig. 11. Three classes of factors secreted by astrocytes to regulate synapse formation. A) Type I, like thrombospondins, results in formation of synapses that are structurally normal, but post-synaptically silent. B) Type II, like cholesterol, increase pre-synaptic activities and increases neurotransmitter releases. C) Type III, which are yet to be identified, increases post-synaptic receptors and convert silent synapses to functional ones. *Adopted from Eroglu et al [49].*

Glia are also is known to play a role during injury to the nervous system, a function that may be relevant in injuries such as viral infection. When insults occur to the

nervous system, astrocytes revert to an immature state and express molecules that alter synaptic formations [49]. In one study, production of proteins TSP1 and TSP2 were shown to be increased in astrocytes after traumatic brain injury and ischemic stroke[49, 59]. In mice, TSP1 and TSP2 were shown in to be required for functional recovery after stroke, since TSP1/2-deficient mice showed impaired motor recovery, synaptic density and axon pruning [60].

Given the gamut of important functions glia are known to play in both the developing and developed nervous system, it is not a surprising observation that infection of underlying astrocytes can result in bystander attenuation of synaptic activity and that it is reasonable to infer that the changes in astrocytes calcium physiology observed in the current experiments could play a role in the pathogenesis of congenital CMV infection. But given that the experiments were performed in-vitro, the true relevance of these findings in-vivo can only be speculated at this point. Further experiments that could be performed would include trying to replicate these findings in-vivo, by infecting embryonic mice in-utero with MCMV. The technical difficulty of performing calcium imaging of live brain slices will have to be overcome. Primarily, confocal microscopy would have to be used to perform imaging on slices. However, excitation of 340 and 380nm is generally not achieved using the laser available in common confocal microscopy. Hence, the Fura-2 calcium indicator cannot be used. Technical modifications to standard confocal microscopic set-up are also needed to alternate excitation or emission spectrum in order to accommodate ratiometric dyes. Obtaining clear images with large number of cells in a field of view is also

dramatically more difficult in live brain slices, making the collection of large amount

of data for quantitative comparison of calcium level much more time-consuming and

resource demanding.

References

1. Cheeran, M.C., J.R. Lokensgard, and M.R. Schleiss, *Neuropathogenesis of congenital cytomegalovirus infection: disease mechanisms and prospects for intervention.* Clin Microbiol Rev, 2009. **22**(1): p. 99-126, Table of Contents.
2. James, S.H., D.W. Kimberlin, and R.J. Whitley, *Antiviral therapy for herpesvirus central nervous system infections: neonatal herpes simplex virus infection, herpes simplex encephalitis, and congenital cytomegalovirus infection.* Antiviral Res, 2009. **83**(3): p. 207-13.
3. Lazzarotto, T., et al., *New advances in the diagnosis of congenital cytomegalovirus infection.* J Clin Virol, 2008. **41**(3): p. 192-7.
4. Alford, C.A., et al., *Congenital and perinatal cytomegalovirus infections.* Rev Infect Dis, 1990. **12 Suppl 7**: p. S745-53.
5. Fowler, K.B., et al., *The outcome of congenital cytomegalovirus infection in relation to maternal antibody status.* N Engl J Med, 1992. **326**(10): p. 663-7.
6. Kenneson, A. and M.J. Cannon, *Review and meta-analysis of the epidemiology of congenital cytomegalovirus (CMV) infection.* Rev Med Virol, 2007. **17**(4): p. 253-76.
7. Boppana, S.B., et al., *Symptomatic congenital cytomegalovirus infection in infants born to mothers with preexisting immunity to cytomegalovirus.* Pediatrics, 1999. **104**(1 Pt 1): p. 55-60.
8. Gaytant, M.A., et al., *Congenital cytomegalovirus infection after recurrent infection: case reports and review of the literature.* Eur J Pediatr, 2003. **162**(4): p. 248-53.
9. Staras, S.A., et al., *Seroprevalence of cytomegalovirus infection in the United States, 1988-1994.* Clin Infect Dis, 2006. **43**(9): p. 1143-51.
10. Cannon, M.J. and K.F. Davis, *Washing our hands of the congenital cytomegalovirus disease epidemic.* BMC Public Health, 2005. **5**: p. 70.
11. Eggers, M., U. Bader, and G. Enders, *Combination of microneutralization and avidity assays: improved diagnosis of recent primary human cytomegalovirus infection in single serum sample of second trimester pregnancy.* J Med Virol, 2000. **60**(3): p. 324-30.
12. Lazzarotto, T., et al., *Avidity of immunoglobulin G directed against human cytomegalovirus during primary and secondary infections in immunocompetent and immunocompromised subjects.* Clin Diagn Lab Immunol, 1997. **4**(4): p. 469-73.
13. Baccard-Longere, M., et al., *Multicenter evaluation of a rapid and convenient method for determination of cytomegalovirus immunoglobulin G avidity.* Clin Diagn Lab Immunol, 2001. **8**(2): p. 429-31.
14. Bodeus, M., D. Beulne, and P. Goubau, *Ability of three IgG-avidity assays to exclude recent cytomegalovirus infection.* Eur J Clin Microbiol Infect Dis, 2001. **20**(4): p. 248-52.
15. Revello, M.G., G. Gorini, and G. Gerna, *Clinical evaluation of a chemiluminescence immunoassay for determination of immunoglobulin g avidity to human cytomegalovirus.* Clin Diagn Lab Immunol, 2004. **11**(4): p. 801-5.

16.   Pass, R.F., *Congenital cytomegalovirus infection and hearing loss.* Herpes, 2005. **12**(2): p. 50-5.

17.   Hicks, T., et al., *Congenital cytomegalovirus infection and neonatal auditory screening.* J Pediatr, 1993. **123**(5): p. 779-82.

18.   Dahle, A.J., et al., *Longitudinal investigation of hearing disorders in children with congenital cytomegalovirus.* J Am Acad Audiol, 2000. **11**(5): p. 283-90.

19.   Williamson, W.D., et al., *Asymptomatic congenital cytomegalovirus infection. Audiologic, neuroradiologic, and neurodevelopmental abnormalities during the first year.* Am J Dis Child, 1990. **144**(12): p. 1365-8.

20.   Paredes, R.M., et al., *Chemical calcium indicators.* Methods, 2008. **46**(3): p. 143-51.

21.   van Den Pol, A.N., et al., *Cytomegalovirus cell tropism, replication, and gene transfer in brain.* J Neurosci, 1999. **19**(24): p. 10948-65.

22.   Auld, D.S. and R. Robitaille, *Glial cells and neurotransmission: an inclusive view of synaptic function.* Neuron, 2003. **40**(2): p. 389-400.

23.   Araque, A. and G. Perea, *Glial modulation of synaptic transmission in culture.* Glia, 2004. **47**(3): p. 241-8.

24.   Schipke, C.G. and H. Kettenmann, *Astrocyte responses to neuronal activity.* Glia, 2004. **47**(3): p. 226-32.

25.   Araque, A., et al., *Synaptically released acetylcholine evokes Ca2+ elevations in astrocytes in hippocampal slices.* J Neurosci, 2002. **22**(7): p. 2443-50.

26.   Nedergaard, M., B. Ransom, and S.A. Goldman, *New roles for astrocytes: redefining the functional architecture of the brain.* Trends Neurosci, 2003. **26**(10): p. 523-30.

27.   Porter, J.T. and K.D. McCarthy, *Hippocampal astrocytes in situ respond to glutamate released from synaptic terminals.* J Neurosci, 1996. **16**(16): p. 5073-81.

28.   van den Pol, A.N., S.M. Finkbeiner, and A.H. Cornell-Bell, *Calcium excitability and oscillations in suprachiasmatic nucleus neurons and glia in vitro.* J Neurosci, 1992. **12**(7): p. 2648-64.

29.   Charles, A.C., *Glia-neuron intercellular calcium signaling.* Dev Neurosci, 1994. **16**(3-4): p. 196-206.

30.   Pasti, L., et al., *Intracellular calcium oscillations in astrocytes: a highly plastic, bidirectional form of communication between neurons and astrocytes in situ.* J Neurosci, 1997. **17**(20): p. 7817-30.

31.   Anderson, C.M., J.P. Bergher, and R.A. Swanson, *ATP-induced ATP release from astrocytes.* J Neurochem, 2004. **88**(1): p. 246-56.

32.   Cornell-Bell, A.H. and S.M. Finkbeiner, *Ca2+ waves in astrocytes.* Cell Calcium, 1991. **12**(2-3): p. 185-204.

33.   Cornell-Bell, A.H., et al., *Glutamate induces calcium waves in cultured astrocytes: long-range glial signaling.* Science, 1990. **247**(4941): p. 470-3.

34.   Cotrina, M.L., et al., *ATP-mediated glia signaling.* J Neurosci, 2000. **20**(8): p. 2835-44.

35.   Guthrie, P.B., et al., *ATP released from astrocytes mediates glial calcium waves.* J Neurosci, 1999. **19**(2): p. 520-8.

36.   Kim, W.T., M.G. Rioult, and A.H. Cornell-Bell, *Glutamate-induced calcium signaling in astrocytes.* Glia, 1994. **11**(2): p. 173-84.

37. Charles, A.C., et al., *Intercellular signaling in glial cells: calcium waves and oscillations in response to mechanical stimulation and glutamate.* Neuron, 1991. **6**(6): p. 983-92.

38. Newman, E.A. and K.R. Zahs, *Calcium waves in retinal glial cells.* Science, 1997. **275**(5301): p. 844-7.

39. Araque, A., G. Carmignoto, and P.G. Haydon, *Dynamic signaling between astrocytes and neurons.* Annu Rev Physiol, 2001. **63**: p. 795-813.

40. Araque, A., et al., *Tripartite synapses: glia, the unacknowledged partner.* Trends Neurosci, 1999. **22**(5): p. 208-15.

41. Fields, R.D. and G. Burnstock, *Purinergic signalling in neuron-glia interactions.* Nat Rev Neurosci, 2006. **7**(6): p. 423-36.

42. Perea, G. and A. Araque, *Synaptic regulation of the astrocyte calcium signal.* J Neural Transm, 2005. **112**(1): p. 127-35.

43. Nokta, M., et al., *Ca2+ responses in cytomegalovirus-infected fibroblasts of human origin.* Virology, 1987. **157**(2): p. 259-67.

44. van den Pol, A.N., J.D. Reuter, and J.G. Santarelli, *Enhanced cytomegalovirus infection of developing brain independent of the adaptive immune system.* J Virol, 2002. **76**(17): p. 8842-54.

45. Fields, R.D. and B. Stevens, *ATP: an extracellular signaling molecule between neurons and glia.* Trends Neurosci, 2000. **23**(12): p. 625-33.

46. Parpura, V., et al., *Glutamate-mediated astrocyte-neuron signalling.* Nature, 1994. **369**(6483): p. 744-7.

47. Suadicani, S.O., C.F. Brosnan, and E. Scemes, *P2X7 receptors mediate ATP release and amplification of astrocytic intercellular Ca2+ signaling.* J Neurosci, 2006. **26**(5): p. 1378-85.

48. Larter, R. and M.G. Craig, *Glutamate-induced glutamate release: a proposed mechanism for calcium bursting in astrocytes.* Chaos, 2005. **15**(4): p. 047511.

49. Eroglu, C. and B.A. Barres, *Regulation of synaptic connectivity by glia.* Nature, 2010. **468**(7321): p. 223-31.

50. Chittajallu, R., A. Aguirre, and V. Gallo, *NG2-positive cells in the mouse white and grey matter display distinct physiological properties.* J Physiol, 2004. **561**(Pt 1): p. 109-22.

51. Lin, S.C. and D.E. Bergles, *Physiological characteristics of NG2-expressing glial cells.* J Neurocytol, 2002. **31**(6-7): p. 537-49.

52. Bergles, D.E., et al., *Glutamatergic synapses on oligodendrocyte precursor cells in the hippocampus.* Nature, 2000. **405**(6783): p. 187-91.

53. Lin, S.C., et al., *Climbing fiber innervation of NG2-expressing glia in the mammalian cerebellum.* Neuron, 2005. **46**(5): p. 773-85.

54. De Biase, L.M., A. Nishiyama, and D.E. Bergles, *Excitability and synaptic communication within the oligodendrocyte lineage.* J Neurosci, 2010. **30**(10): p. 3600-11.

55. Lin, S.C. and D.E. Bergles, *Synaptic signaling between GABAergic interneurons and oligodendrocyte precursor cells in the hippocampus.* Nat Neurosci, 2004. **7**(1): p. 24-32.

56. Pfrieger, F.W. and B.A. Barres, *Synaptic efficacy enhanced by glial cells in vitro.* Science, 1997. **277**(5332): p. 1684-7.

57.   Ullian, E.M., et al., *Control of synapse number by glia.* Science, 2001. **291**(5504): p. 657-61.
58.   Barres, B.A., *The mystery and magic of glia: a perspective on their roles in health and disease.* Neuron, 2008. **60**(3): p. 430-40.
59.   Lin, T.N., et al., *Differential regulation of thrombospondin-1 and thrombospondin-2 after focal cerebral ischemia/reperfusion.* Stroke, 2003. **34**(1): p. 177-86.
60.   Liauw, J., et al., *Thrombospondins 1 and 2 are necessary for synaptic plasticity and functional recovery after stroke.* J Cereb Blood Flow Metab, 2008. **28**(10): p. 1722-32.